

CDI: Blind Image Restoration Fidelity Evaluation based on Consistency with Degraded Image

Xiaojun Tang^{*,†}, Jingru Wang^{*}, Guangwei Huang, Guannan Chen, Rui Zheng
Lian Huai, Yuyu Liu, Xingqun Jiang
BOE Technology Group Co., Ltd, Beijing, China

{tangxiaojun, wangjingru, huangguangwei, chenguannan, zhengr,
huailian, liuyuyu, jiangxingqun}@boe.com.cn

Abstract

Recent advancements in Blind Image Restoration (BIR) methods, based on Generative Adversarial Networks and Diffusion Models, have significantly improved visual quality. However, they present significant challenges for Image Quality Assessment (IQA), as the existing Full-Reference IQA methods often rate images with high perceptual quality poorly. In this paper, we reassess the Solution Non-Uniqueness and Degradation Indeterminacy issues of BIR, and propose constructing a specific BIR IQA system. Instead of directly comparing a restored image with a reference image, the BIR IQA evaluates fidelity by calculating the Consistency with Degraded Image (CDI). Specifically, we propose a wavelet domain Reference Guided CDI algorithm, which can acquire the consistency with a degraded image for various types without requiring knowledge of degradation parameters. The supported degradation types include down sampling, blur, noise, JPEG and complex combined degradations etc. In addition, we propose a Reference Agnostic CDI, enabling BIR fidelity evaluation without reference images. Finally, in order to validate the rationality of CDI, we create a new Degraded Images Switch Display Comparison Dataset (DISDCD) for subjective evaluation of BIR fidelity. Experiments conducted on DISDCD verify that CDI is markedly superior to common Full Reference IQA methods for BIR fidelity evaluation. The source code and the DISDCD dataset will be publicly available shortly.

1. Introduction

Traditional Image Restoration algorithms, including image denoising [16, 57], deblurring [18, 53] and super-resolution

^{*}The top two authors contributed equally to this work and should be considered co-first authors.

[†]Corresponding author.

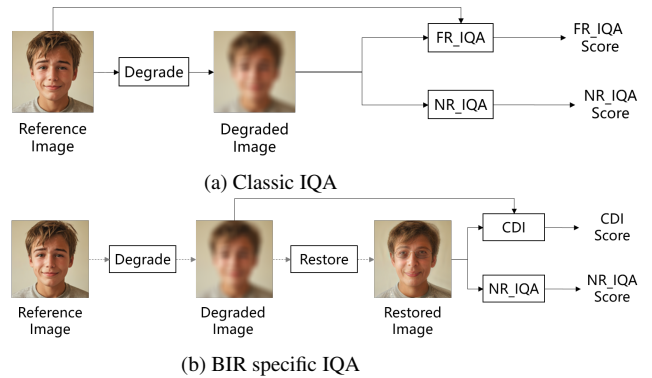


Figure 1. (a) Classic IQA includes Full Reference IQA and No Reference IQA. (b) The proposed BIR specific IQA applies Consistency with Degraded Image instead of Full Reference IQA

[10, 27, 61] *et al.*, are designed and trained to restore images specifically with known degradation. However, they generally have weak generalization abilities and struggle with restoring degraded images with complex or unknown degradation. In recent years, Blind Image Restoration (BIR) [24, 39, 43] has emerged as a promising research direction. It aims at reconstructing general images degraded by unknown, real-world factors. BIR is designed to handle a variety of degradation types, making it a promising solution for numerous applications.

Challenge of BIR IQA Evaluation. The most recent BIR methods based on Generative Adversarial Networks (GANs) [39, 54] and Diffusion Models (DMs) [24, 38, 43], have achieved significant improvement in visual performance. Nonetheless, they pose substantial challenges for Image Quality Assessment (IQA). By utilizing the image generation ability of GANs and DMs, BIR algorithms are able to generate visually realistic details and textures. However, as the visual quality of BIR restored images improves, the scores [11, 41, 60] of Full Reference IQA (FR_IQA) tend to decrease. These FR_IQA methods have a tendency

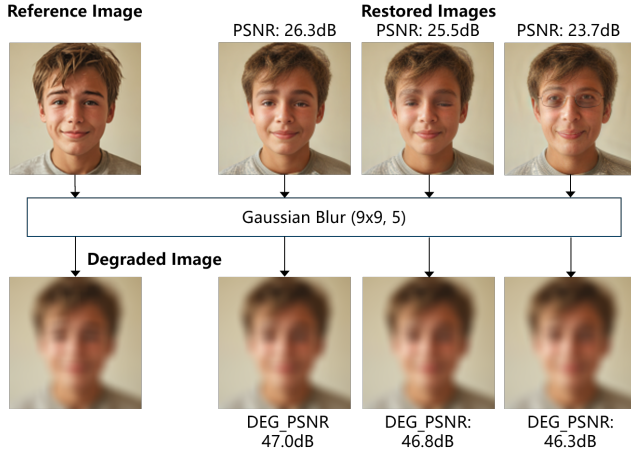


Figure 2. BIR resolution is Non-Unique. It is impossible to determine which one is the Ground Truth reference image using only the degraded image.

to give high scores to blurry restored images, indicating a need for further improvement in their assessment methods.

BIR Solution Non-Uniqueness. The process of image degradation often leads to the loss of image information. As its inverse process, image restoration is an ill-posed problem. Figure.2 shows that the BIR usually has an infinite number of solutions. Given an image blurred with a Gaussian filter, three visually distinct images are generated using existing BIR algorithms (with DEG_PSNR maximization gradient adjustment). The first image has different hair textures, the second one features closed eyes, and the third one exhibits an individual wearing glasses. In addition to the visual differences, all three images have low PSNR values. However, once the same Gaussian blur is applied to them, they appear near-identical to the degraded image ($DEG_PSNR > 46dB$), indicating that they are all valid solutions. In fact, the Ground Truth reference image is merely one of these many solutions. Theoretically, it is impossible to definitively determine which one is the Ground Truth reference image using only the degraded image. Note: DEG_PSNR represents the PSNR of Degraded Images, which is the PSNR value of two images subjected to the same degradation operation.

BIR Degradation Indeterminacy. Intuitively, the type of degradation, such as blur, noise, JPEG compression, etc. can be roughly identified through the degraded image, but the accurate degradation parameters cannot be determined. As shown in Figure.3, given a blurry image degraded by $\sigma = 1.0$ Gaussian kernel, we apply image deblurring with different σ values and generate three restored images with significant contrast differences. However, after Gaussian blurring with different σ parameters, all the images become almost identical to the degraded images, indicating that they

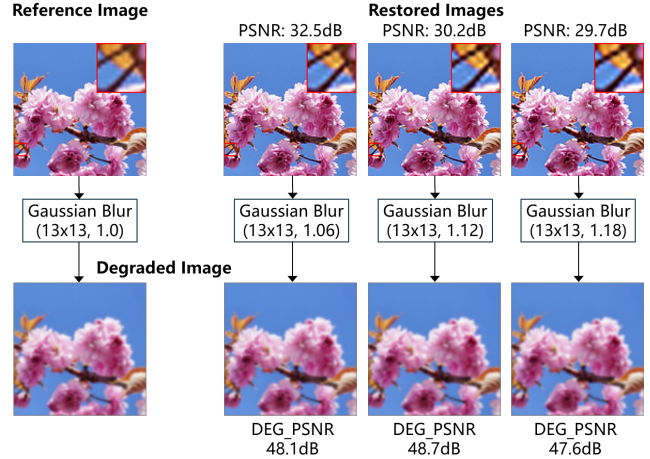


Figure 3. Given the indeterminate nature of BIR degradation, it's impossible to accurately determine the degradation parameters solely through an examination of the degraded image.

are all correct solutions. Therefore, it is impossible to accurately determine degradation parameters based on the degraded image alone.

BIR Specific IQA. Figure.1a illustrates structure of the classic Image Quality Assessment (IQA) [3, 11, 26, 41, 45, 58, 60] system. In this system, the degradation system is the object of evaluation. Full Reference IQA (FR_IQA) is designed for estimating the pixel or perceptual similarity between the given degraded images and their corresponding reference images. For the No Reference IQA (NR_IQA) evaluation methodology, only the degraded images are provided, and no reference images are available.

Contrary to Classic IQA, BIR IQA evaluates the image quality of restored images in stead of degraded images. In this context, the restoration system becomes the object of evaluation rather than the degradation system. BIR IQA should be evaluated from two different aspects. One is Consistency with Degraded Image (CDI), the other is Perceptual Quality. Figure.1b shows the proposed BIR specific IQA, which evaluates CDI by comparing restored images with degraded images, and evaluates Perceptual Quality with NR_IQA.

Since that the resolution in BIR is Non-Unique and the reference image is indeterminate, comparing the restored image with the reference image as done in FR_IQA isn't rational. The intuitive approach involves applying the same degradation to the restored image and then comparing it with the reference image's degraded version. On the other hand, considering that BIR degradation is indeterminate, the degradation function applied to the restored image can differ from the function used on the degraded image.

Consistency with Degraded Image (CDI). It is not feasible to simply use the same degradation function to de-

grade the restored image, and calculate the DEG_PSNR as CDI index. First, in BIR, the degradation function is assumed to be unknown, thus DEG_PSNR cannot be applied to scenarios where the reference image is unavailable. Second, the degradation noise might be uncontrollable, such as JPEG noise, and will result in a mismatch between the degraded restored image and the degraded reference image. In addition, for additive noise degradation, the noise in the degraded restored image is directly subtracted, so the DEG_PSNR is simplified to a conventional PSNR.

In this paper, we concentrate on CDI calculation and propose a wavelet-based Reference Guided CDI (RGCDI) algorithm, which splits the degraded image into the attenuated image and additive noise images as shown in Figure.6. We further convert signal loss caused by the noise into equivalent image attenuation to guarantee accurate BIR CDI calculation. Besides, we train a Wavelet Attenuation Extraction Net (WAENet) to simulate the extraction of attenuated images present in RGCDI, thereby achieving the Reference Agnostic CDI (RACDI) calculation. Finally, we build a new Degraded Images Switch Display Comparison Dataset (DISDCD) for BIR fidelity subjective evaluation. DISDCD uses an alternating display method to enable data annotator to measure the differences between degraded images more accurately. This dataset serves as an effective benchmark for CDI evaluation.

The contribution of this work is summarized as follows:

- We revisit the Solution Non-Uniqueness and Degradation Indeterminacy issue associated with BIR and suggest to build an IQA system specifically designed for BIR.
- A wavelet-based Reference Guided CDI (RGCDI) algorithm is proposed, which can evaluate the consistency with degraded image for various types of degradations without knowing degradation parameters.
- We train a general Wavelet Attenuation Extraction Net (WAENet), achieving the Reference Agnostic CDI (RACDI) calculation.
- A new Degraded Images Switch Display Comparison Dataset (DISDCD) is built as BIR CDI benchmark. Experiments on DISDCD verify that the proposed RGCDI and RACDI are consistent with subjective evaluation results.

2. Related work

Full-Reference Image Quality Assessment (FR_IQA) methods, such as PSNR, SSIM [41], LPIPS [60], DISTS [11] *et al.*, measure the similarity between two images. The early FR_IQA methods [41] mainly calculate pixel level similarity, while the recent FR_IQA methods [11, 60] focus on perceptual similarity. FR_IQA methods are widely used in the evaluation of image/video coding, communication and images restoration quality. However, for restored

images quality assessment, FR_IQA method only compares the restored image with the reference image, without taking the degraded image into account.

No-Reference Image Quality Assessment (NR_IQA) methods, for instance, NIQE [58], MANIQA [45], BRISQUE [26], and PI [3] *et al.*, are proposed to assess image quality without a reference image. NR_IQA methods mainly evaluate image perceptual quality, but cannot describe image fidelity.

Reduced-Reference Image Quality Assessment (RR_IQA) methods, such as RRED [36], OSV [42], evaluate image quality by comparing partial information of the reference image with the degraded image. Similar to FR_IQA methods, RR_IQA methods also ignore degraded images.

Plug-and-play Image Restoration includes a series of new promising image restoration methods [9, 13, 40, 56, 63]. Generally, they adopt a two step image degradation modeling and solve image restoration problems by calculating a Maximum A Posterior (MAP). Then, the image restoration target is split into two items, minimizing the error of degraded images and maximizing the prior probability of image. The former can be regarded as a good fidelity quantitative evaluation index. However, existing Plug-and-play methods depend on known degradation operations, cannot be used in Blind Image Restoration. In this paper, the proposed Consistency with Degraded Image methods do not rely on degradation information and can be used for BIR fidelity evaluation.

3. Reference Guided CDI (RGCDI)

For Synthetic Image Restoration datasets, reference images are available and can be used to assist in the calculation of CDI. In this section, we propose a wavelet domain Reference Guided CDI algorithm. Figure.4a illustrates the system structure. The main idea is to remove random noise from the degraded image, and get the attenuated reference image with only high-frequency attenuation. The restored image is attenuated accordingly, which is compared with the attenuated reference image to calculate CDI.

The reference image I_x , degraded image I_y and restored image I_t are converted to wavelet domain by 2 dimensional Discrete Wavelet Transform (DWT). The wavelet coefficients are denoted as x , y and t respectively. The Wavelet Noise Splitting (WNS) module splits y into $\mu_A x$ and n . The Wavelet Noise Equivalent Attenuation (WNEA) module further attenuates $\mu_A x$ to $\mu_N \mu_A x$. The Wavelet Attenuation Matching (WAM) module adaptively attenuates t to best match $\mu_N \mu_A x$, and obtains $\mu_M t$. Finally, $\mu_N \mu_A x$ and $\mu_M t$ are converted back to pixel domain by 2 dimensional Inverse Discrete Wavelet Transform (IDWT). The corresponding attenuation images are denoted as $I_{\tilde{y}}$ and $I_{\tilde{t}}$ respectively. Then we can calculate PSNR for $I_{\tilde{y}}$ and $I_{\tilde{t}}$ and

get the $RGCDI_PSNR$ score.

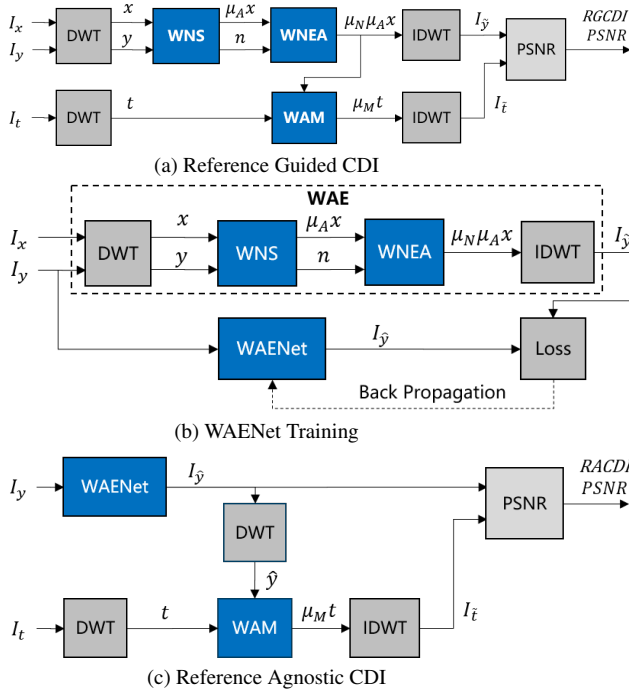


Figure 4. (a) Reference Guided CDI calculates the wavelet domain attenuated reference image and restored image, and obtains $RGCDI_PSNR$ by comparing the attenuated images. (b) WAENet is trained to predict the attenuated reference image from the degraded image. (c) Reference Agnostic CDI calculates $RACDI_PSNR$ without reference images.

3.1. Two Step Image Degradation Modeling

Image degradation usually includes high-frequency detail loss and noise addition, and can be modeled by the general two step image degradation [56, 63] $I_y = \Gamma(I_x) + I_n$, where Γ is a data attenuation operation and I_n is assumed to be additive noise, as Figure.5 illustrated.

Similarly, in wavelet domain, image degradation can also be generally modeled by the two step wavelet degradation [40, 56, 63] as formula.1 shows, in which μ_A is the attenuation coefficient, n is assumed to be additive white Gaussian noise of standard deviation σ_n , and i is the block index of wavelet sub-band. The image wavelet coefficient $x[i]$ can be modeled using Gaussian Scale Mixture (GSM) [37], as expressed in formula.2, where $s[i]$ is an RF of positive scalars and $u[i]$ is a Gaussian vector RF with mean zero and covariance C_u .

This wavelet domain degradation model can well simulate the attenuation and noise of high-frequency signals with different frequencies, and can capture the effects of real-world distortions adequately in terms of the perceptual annoyance [34].

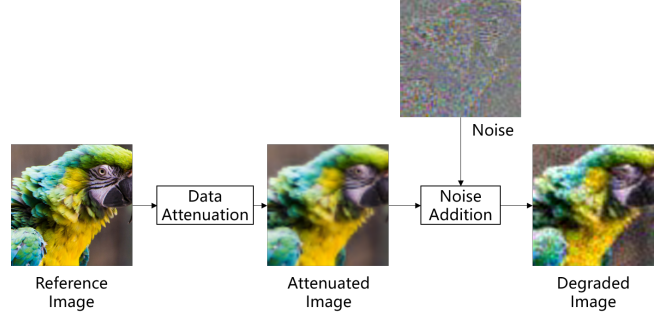


Figure 5. Two Step Image Degradation Modeling

$$y[i] = \mu_A x[i] + n[i] \quad (1)$$

$$x[i] = s[i] u[i] \quad (2)$$

3.2. Wavelet Noise Splitting (WNS)

According to formula.1, we want to split $y[i]$ into $\mu_A x[i]$ and $n[i]$. Given the reference $x[i]$, the noise splitting is easy to solve in view of the fact that $COV(n[i], x[i]) = 0$ (x and n are independent in probability)[34]. (See formula.3, 4)

$$\mu_A = COV(y, x) / COV(x, x) \quad (3)$$

$$n[i] = y[i] - \mu_A x[i] \quad (4)$$

The standard deviation σ_n can also be estimated as formula.5 illustrated [34].

$$\sigma_n^2[i] = COV(y[i], y[i]) - \mu_A COV(y[i], x[i]) \quad (5)$$

Figure.6 demonstrates split images of various degradations. Gaussian Blur and Down Sampling have large high-frequency attenuation while little noise. Gaussian Noise is mainly composed of additional noise, with little attenuation. JPEG and Combined Degradation [39] have both attenuation and noise.

3.3. Wavelet Noise Equivalent Attenuation (WNEA)

The μ_A attenuation leads to the loss of high-frequency signals, and similarly, additive noise n can also result in the loss of image signals. Therefore, the CDI calculation should take the influence of n into account.

Considering the wavelet domain additive noise degradation shown in formula.6, the solution $\hat{x}[i]$ can be obtained by solving the Maximum A Posterior (MAP) from the Bayesian perspective [40, 56, 63]. In formula.7,

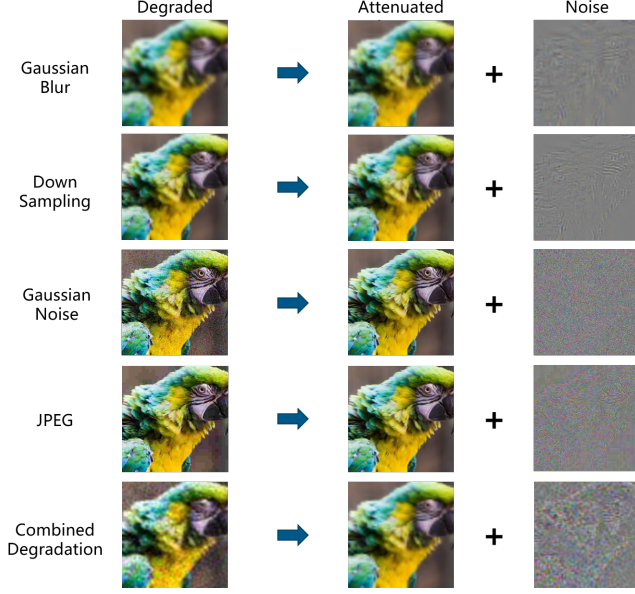


Figure 6. Example sample images of Wavelet Noise Splitting

$\log(p(y[i] | x[i]))$ represents the log-likelihood of observation $y[i]$, $\log(p(x[i]))$ represents the prior of reference image $x[i]$. The derivation of formula.7 utilizes the Gaussian probability distributions of $n[i]$ and $x[i]$.

$$y[i] = x[i] + n[i] \quad (6)$$

$$\begin{aligned} \hat{x}[i] &= \arg \max_{x[i]} \log(p(y[i] | x[i])) + \log(p(x[i])) \\ &= \arg \min_{x[i]} \frac{1}{\sigma_n^2} \|y[i] - x[i]\|^2 + x[i]^T C_x^{-1} x[i] \quad (7) \\ &= (I + \sigma_n^2 C_x^{-1})^{-1} y[i] \end{aligned}$$

Since $x[i]$ in formula.6 has been attenuated by μ_A , the covariance matrix C_x needs to be multiplied by μ_A^2 (See formula.8). The image signal loss caused by $n[i]$ can be equivalent to μ_N attenuation shown by formula.9. In extreme cases, when n is much greater than x , μ_N approaches 0.

$$C_x = COV(\mu_A x, \mu_A x) = \mu_A^2 COV(x, x) \quad (8)$$

$$\mu_N = \left(I + \frac{\sigma_n^2}{\mu_A^2} COV(x, x)^{-1} \right)^{-1} \quad (9)$$

3.4. Wavelet Attenuation Matching (WAM)

In order to compare the restored image I_t with the attenuated image $I_{\bar{y}}$, I_t should be attenuated accordingly. Considering that BIR degradation is indeterminate (Figure.3),

the attenuation coefficients of I_t can also be different from $\mu_N \mu_A$, which can be calculated by minimizing the squared error as formula.10 shows.

$$\begin{aligned} \mu_M &= \arg \min_{\mu_M} \|\mu_M t - \mu_N \mu_A x\| \\ &= COV(t, \mu_N \mu_A x) / COV(t, t) \end{aligned} \quad (10)$$

Subsequently, the *RGCDI_PSNR* score can be computed using formula.11, where $I_{\bar{y}}$ is the IDWT transformation of $\mu_M t$.

$$RGCDI_PSNR(I_t, I_y) = PSNR(I_{\bar{t}}, I_{\bar{y}}) \quad (11)$$

3.5. RGCDI Property Analysis

In this section, we combine the above WNS and WNEA (named Wavelet Attenuation Extraction (WAE)), $WAE(I_x, I_y) = I_{\bar{y}}$. The properties of WAE and RGCDI are illustrated as follows.

Idempotency. Multiple WAE operations are equivalent to a single one.

$$\begin{aligned} WAE(I_x, I_y) &= WAE(I_x, WAE(I_x, I_y)) \\ &= WAE(WAE(I_x, I_y), I_y) \end{aligned} \quad (12)$$

WAE and Degradation Cascade Exchangeability. The WAE of cascading multiple degradations is equivalent to cascading multiple WAEs of a single degradation.

$$\begin{aligned} WAE(I_x, D_2(D_1(I_x))) \\ &= WAE(WAE(I_x, D_1(I_x)), D_2(D_1(I_x))) \end{aligned} \quad (13)$$

RGCDI_PSNR \geq PSNR (Conditional). In general, the attenuation coefficients satisfy $0 \leq \mu_N \mu_A \leq 1$, and the differences between degraded images is smaller than that of the original images.

4. Reference Agnostic CDI (RACDI)

In the RGCDI structure, the calculation of $I_{\bar{y}}$ depends on the reference images, which cannot be obtained in real-world image restoration. We proposed a Reference Agnostic CDI algorithm and achieved CDI calculation without reference images. By observation, it can be found that the WAE operation removes noise from the degraded image I_y and converts the noise into equivalent image attenuation μ_N . The output image $I_{\bar{y}}$ is a denoised and blurred version of I_y . This inspires us to adopt a denoising model to directly convert I_y into $I_{\bar{y}}$.

As Figure.4b shows, paired $(I_t, I_{\bar{t}})$ training images of various types of degradations can be generated through the WAE module. After end-to-end training, the Wavelet Attenuation Extraction Net (WAENet) is able to predict $I_{\bar{t}}$ from

I_t generally. Many off the shelf denoise models, such as SCUNet [55] and Restormer [50] *et al.*, can be used as the candidate WAENet. In Figure.4c, the output of WAENet is denoted as $I_{\hat{t}}$. We replace $I_{\hat{t}}$ of the RGCDI structure with $I_{\hat{t}}$, so that $RACDI_PSNR$ scores can be calculated.

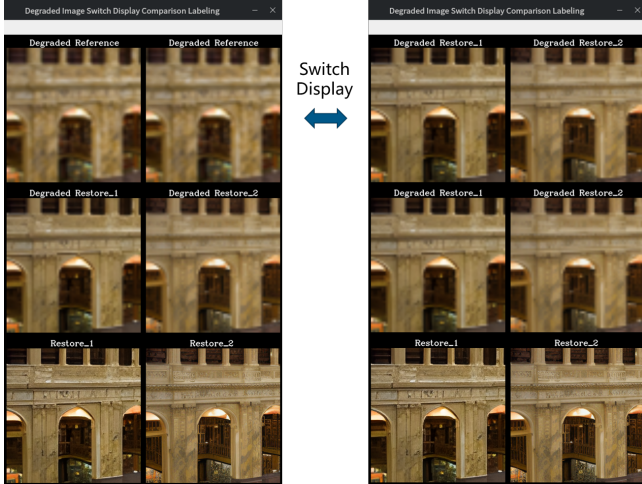


Figure 7. DISDCD annotation interface

5. Degraded Images Switch Display Comparison Dataset (DISDCD)

Many IQA datasets have been proposed for evaluating IQA methods, such as LIVE [35], CSIQ [17], TID2008 [31], TID2013 [30], PieAPP [32], and BAPPS [59], QADS [62], PIPAL [14]. These datasets provide subjective scores for various types of distorted images, including restored images from image restoration algorithms. However, the existing datasets compare the restored images with reference images, ignoring the degraded images prior to image restoration.

In order to evaluate the proposed RGCDI and RACDI methods, we build a new Degraded Images Switch Display Comparison Dataset (DISDCD). The DISDCD contains restored images of 4 types of degradations, including Down Sampling (4x), Gaussian noise ($\sigma = 50$), JPEG (QF10) and combined degradation (Real-ESRGAN second-order degradation [39]). Each degradation type contains 100 degraded images from DIV2K [2], and 200 restored images. BIR restoration algorithms include BSRGAN [54], Real-ESRGAN [39], LDL [23], DASR [22], FeMaSR [4], LDM [33], StableSR [38], ResShift [49], PASD [46], Diff-BIR [24], SeeSR [43].

The DISDCD adopts the Two Alternative Forced Choice (2AFC) [60] for the subjective judgment. We select a reference image I_x , apply the degradation operation on it, and obtain the degraded image I_y . Then we randomly select two BIR algorithms to produce restored images I_{t1} , I_{t2} from I_y .

In order to better observe the differences between degraded images, We apply the same degradation operation on I_{t1} and I_{t2} , and obtains I_{y1} and I_{y2} . We then ask a human which is closer to I_y , and record response $h \in \{0, 1\}$. It should be noted that when generating Gaussian noise in the degradation operation, a fixed random seed is required to keep the noise unchanged and ensure the consistency of the noise degraded images.

In order to better distinguish the small differences between degraded images. We apply the Double-Stimulus Continuous Quality-Scale (DSCQS) method from ITU-R BT.500-15 [1] in the subjectivity judgment. Figure.7 illustrates the DISDCD annotation interface. The top row displays two identical degraded images I_y . The middle row displays two degraded images I_{y1} and I_{y2} . The bottom row displays two restored images I_{t1} and I_{t2} . The participant can use buttons to repeatedly switch the first row display images from I_y to I_{y1} , I_{y2} , until they can give a clear judgment.

6. Experiments

In this section, We do experiments to verify the effectiveness of the proposed RGCDI and RACDI. Section 6.1 compares the proposed methods with common FR IQA methods on DISDCD dataset. Experimental results show that the 2AFC scores of RGCDI and RACDI is much higher than others. Section 6.2 compares 4 candidate WAENet backbone networks on 6 Image Restoration tasks. Experimental results show that the SCUNet has the best performance. Section 6.3 tests the errors of RACDI.PSNR relative to RGCDI.PSNR. Experimental results show that the errors of Motion Blur, ClassicSR, Gaussian Noise, Real Noise and Blind Restoration are less than 3dB, and the maximum mean error of JPEG Restoration reaches 6.13dB.

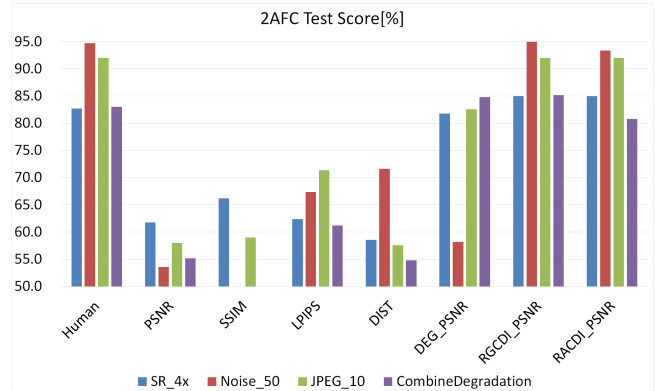


Figure 8. Evaluation on DISDCD. The proposed RGCDI and RACDI algorithms have significantly higher 2AFC test scores, close to subjective judgments.

Method	Set5		Set14		BSD100		Manga109		Urban100	
	x2	x4	x2	x4	x2	x4	x2	x4	x2	x4
SCUNet	40.00	39.84	39.51	38.82	39.77	39.61	39.85	39.38	39.23	39.01
Restormer	40.00	39.56	39.51	38.77	39.74	39.55	39.81	39.25	39.15	38.86
CGNet	37.50	35.33	38.09	34.44	39.67	39.52	38.64	32.55	38.60	36.47
NAFNet	38.28	36.01	38.29	35.13	39.68	39.53	38.10	33.30	38.64	36.44

Table 1. WAnet Backbone Comparison on **ClassicSR** validation sets ($PSNR$): SCUNet and Restormer are obviously better than CGNet and NAFNet.

Method	CBSD68			Kodak24			McMaster			Urban100			SIDD
	$\sigma = 15$	$\sigma = 25$	$\sigma = 50$	$\sigma = 15$	$\sigma = 25$	$\sigma = 50$	$\sigma = 15$	$\sigma = 25$	$\sigma = 50$	$\sigma = 15$	$\sigma = 25$	$\sigma = 50$	
SCUNet	37.38	36.40	34.55	38.46	37.78	36.62	38.34	37.38	35.60	36.29	35.48	34.40	36.83
Restormer	37.42	36.47	34.78	38.44	37.81	36.71	38.14	37.17	35.44	36.32	35.60	34.59	37.29
CGNet	36.45	34.60	32.66	38.33	37.69	36.76	37.07	35.55	33.62	35.76	35.09	34.12	36.74
NAFNet	36.41	34.96	33.03	38.34	37.73	36.81	37.08	35.62	33.77	35.80	35.13	34.20	36.82

Table 2. WAnet Backbone Comparison on **Gaussian De-noise** validation sets ($PSNR$): SCUNet and Restormer are slightly better than CGNet and NAFNet.

Method	SCUNet	Restormer	CGNet	NAFNet
GoPro	36.66	36.13	37.11	37.03
HIDE	37.74	36.62	37.40	37.31
RealBlur-J	33.29	33.14	31.86	32.08
RealBlur-R	38.06	38.14	37.86	37.83

Table 3. WAnet Backbone Comparison on **MotionBlur** validation sets ($PSNR$): There is no significant difference in the PSNR scores of all models.

Method	SCUNet	Restormer	CGNet	NAFNet
LIVE1	QF10	32.76	32.64	32.60
	QF20	34.62	34.48	34.37
	QF30	35.32	35.19	35.03
	QF40	35.73	35.57	35.39
BSD500	QF10	33.59	33.47	32.48
	QF20	35.38	35.26	34.36
	QF30	36.07	35.98	35.17
	QF40	36.44	36.36	35.65

Table 4. WAnet Backbone Comparison on **JPEG Restoration** validation sets ($PSNR$): SCUNet is slightly better than other models.

6.1. Evaluation on DISDCD

This experiment compares the proposed RGCDI and RACDI methods with common FR_IQA methods (including PSND, SSIM [41], LPIPS [60], DISTS [11]), DEG_PSNR and Human. DEG_PSNR represents the PSNR score of 2 degraded restored images. The DISDCD validation sets contain 5 pairwise judgments for each sample. As [60] suggests, human accuracy can be calculated as formula.14 shows, where p represent subjective judgment similarity. For example, if there are 4 preferences for I_{t1} and 1 for I_{t2} , $p = 0.8$.



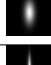
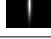
Method	SCUNet	Restormer	CGNet	NAFNet
	$\sigma = 5$	39.20	37.88	35.47
	$\sigma = 10$	37.99	36.64	34.05
	$\sigma = 5$	38.96	38.18	35.48
	$\sigma = 10$	37.34	36.89	34.17
	$\sigma = 5$	39.18	38.40	35.48
	$\sigma = 10$	37.43	36.85	34.07
	$\sigma = 5$	38.44	37.66	34.79
	$\sigma = 10$	36.79	36.24	33.65

Table 5. WAnet Backbone Comparison on **BlindSR** validation sets, use Set14 dataset ($PSNR$): SCUNet is obviously better than other models.

Method	SCUNet	Restormer	CGNet	NAFNet
DIV2K	33.35	33.17	33.72	33.72
CelebA	34.28	34.09	34.62	34.61
DrealSR	32.05	31.96	31.92	31.80
RealSR	30.80	30.60	30.68	30.61

Table 6. WAnet Backbone Comparison on **Blind Restoration** validation sets ($PSNR$): There is no significant difference in the PSNR scores of all models.

$$2AFC_{Human} = p^2 + (1 - p)^2 \quad (14)$$

Similar to [60], We calculated the average 2AFC scores of all subjective judgments as the final 2AFC score. Figure.8 illustrates the evaluation results on DISDCD. The 2AFC scores of PSNR, SSIM, LPIPS, DISTS are all obviously lower. The DEG_PSNR achieves higher scores, except for the Gaussian Noise degradation test, because the DEG_PSNR is simplified to the ordinary PSNR in additive Noise experiments. The proposed RGCDI achieves the highest score, and even some scores exceed the Hu-

		MT-RNN [29]	DMPHN [52]	MIMO-UNet+ [8]	MPRNet [51]	Restormer	GRL-B
Motion Blur		38.01 / 1.60	38.09 / 1.57	38.03 / 1.66	37.86 / 1.76	37.92 / 1.72	37.78 / 1.94
		RCAN [61]	SAN [10]	HAN [27]	IPT [5]	SwinIR [21]	GRL-S [20]
ClassicSR	x2	39.77 / 0.24	39.80 / 0.19	39.77 / 0.23	39.69 / 0.31	39.73 / 0.23	39.67 / 0.34
	x4	39.54 / 0.32	39.61 / 0.28	39.55 / 0.42	39.41 / 0.55	39.47 / 0.43	39.36 / 0.62
		DnCNN [16]	IPT	DRUNet [57]	SwinIR	Restormer	SCUNet
Gaussian Noise	$\sigma = 15$	38.00 / 2.11	-	38.87 / 1.39	39.54 / 1.84	38.81 / 1.20	38.88 / 1.22
	$\sigma = 25$	37.12 / 1.95	-	38.31 / 1.50	39.29 / 2.24	38.26 / 1.28	38.32 / 1.29
	$\sigma = 50$	35.32 / 1.38	34.08 / 2.06	37.30 / 1.44	38.88 / 2.71	37.28 / 1.30	37.32 / 1.28
		AT-BSN(D) [7]	S-Adaptive [19]	SDAP [28]	InvDN [25]	DANet [48]	VDN [47]
Real Noise		39.87 / 0.30	39.94 / 0.14	39.80 / 0.26	39.96 / 0.06	39.95 / 0.06	39.95 / 0.06
		SeeSR [43]	DiffBIR [24]	StableSR [38]	RealESRGAN	BSRGAN [54]	FeMaSR [4]
Blind Restoration		32.95 / 1.63	35.28 / 2.47	30.60 / 1.20	34.14 / 2.30	35.21 / 2.91	35.42 / 2.86
		QGAC [12]	FBCNN [15]	GRL-S	-	-	-
JPEG	QF10	39.42 / 5.83	39.93 / 6.13	39.92 / 5.55	-	-	-
	QF20	39.78 / 4.43	39.98 / 4.44	39.96 / 3.91	-	-	-
	QF30	39.82 / 3.66	39.98 / 3.68	39.96 / 3.13	-	-	-
	QF40	39.85 / 3.26	39.98 / 3.28	39.96 / 2.72	-	-	-

Table 7. **RACDI Test Results:** For each cell of data in this table, the number on the left represents RACDI.PSNR and the number on the right represents the mean error of RACDI.PSNR relative to RGCDI.PSNR. (1) Motion Blur task uses GoPro dataset, Maximum Mean Error 1.94dB, (2) ClassicSR task uses Urban100 dataset, Maximum Mean Error 0.62dB, (3) Gaussian Noise task uses Urban100 dataset, Maximum Mean Error 2.71dB (Note: Official IPT model does not support σ 15, 25), (4) Real Noise task uses SIDD dataset, Maximum Mean Error 0.3dB, (5) Blind Restoration task uses DIV2K dataset, Maximum Mean error 2.91dB, (6) JPEG task uses BSDS500 dataset, Maximum Mean Error 6.13dB

man scores. The scores of proposed RACDI are just slightly lower than that of RGCDI, indicating that the WAENet fits the attenuated image extraction well.

6.2. WAENet Backbone Networks Comparison

In general, the ordinary image restoration model training can only be conducted on one specific image restoration task (such as SR, De-noise, Deblur *et al*). If forced to train on multiple tasks simultaneously, the accuracy of the model would be very low. Different from ordinary image restoration tasks, the WAENet only needs to predict attenuated reference images, which is much easier than predicting clean reference images. Therefore, it is hopeful that we can train a general WAENet for various Image Restoration tasks.

Specifically, we select 6 kinds of image restoration tasks including ClassicSR, BlindSR, MotionBlur, Gaussian De-noise, JPEG Restoration and Blind Restoration [39]. The datasets of ClassicSR include DIV2k, BSD100, Manga109, Urban100, Set14 and Set5; The datasets of Gaussian De-noise include CBSD68, Kodak24, McMaster, Urban100 and SIDD; The datasets of MotionBlur include GoPro, HIDE, RealBlur-J and RealBlur-R; The datasets of JPEG Restoration include LIVE1 and BSD500; The dataset of BlindSR is Set14; The datasets of Blind Restoration include DIV2K, CelebA, DrealSR and RealSR.

We select 4 kinds of off-the-shelf De-noise networks (SCUNet [55], Restormer [50], CGNet [44] and NAFNet [6]) as the candidate WAENet backbone networks. Each model is trained for 300k iterations, and then tested on various validation sets. The experimental results show that the

performance of SCUNet is the best. , Restormer is the second, and the performance of CGNet and NAFNet is relatively lower.

6.3. RACDI Testing

In this experiment, we apply SCUNet as the WAENet backbone network, and test the RACDI on 6 image restoration tasks (ClassicSR, BlindSR, MotionBlur, Gaussian De-noise, JPEG Restoration and Blind Restoration [39]). For the JPEG Restoration task, we select 3 common JPEG Restoration algorithms. For other tasks, we select 6 image restoration algorithms for each task. Table.7 shows that the mean errors of Motion Blur, ClassicSR, Gaussian Noise, Real Noise and Blind Restoration are less than 3dB. The mean errors of JPEG Restoration are higher and the maximum mean error reaches 6.13dB.

7. Conclusion

In this paper, we focus on the fidelity evaluation of Blind Image Restoration (BIR). Following an analysis of BIR’s Solution Non-Uniqueness and Degradation Indeterminacy issues, we propose constructing an IQA system specific to BIR. Additionally, we put forward a wavelet-based Reference Guided CDI (RGCDI) algorithm, which can evaluate consistency of degraded image more accurately. Furthermore, we train a general Wavelet Attenuation Extraction Net (WAENet) to realize Reference Agnostic CDI (RACDI) calculation. Finally, we create a new Degraded Images Switch Display Comparison Dataset (DISDCD), Experiments on DISDCD verify that the proposed RGCDI

and RACDI align with subjective evaluation results. We anticipate the adoption of Consistency with Degraded Image as a fidelity evaluation metric for Blind Image Restoration.

References

- [1] Recommendation itu-r bt.500-15, 2023. 6
- [2] Eirikur Agustsson and Radu Timofte. Ntire 2017 challenge on single image super-resolution: Dataset and study. In *2017 IEEE Conference on Computer Vision and Pattern Recognition Workshops (CVPRW)*, pages 1122–1131, 2017. 6
- [3] Yochai Blau and Tomer Michaeli. The perception-distortion tradeoff. In *2018 IEEE/CVF Conference on Computer Vision and Pattern Recognition*, pages 6228–6237, 2018. 2, 3
- [4] Chaofeng Chen, Xinyu Shi, Yipeng Qin, Xiaoming Li, Xiaoguang Han, Tao Yang, and Shihui Guo. Real-world blind super-resolution via feature matching with implicit high-resolution priors. 2022. 6, 8
- [5] Hanting Chen, Yunhe Wang, Tianyu Guo, Chang Xu, Yiping Deng, Zhenhua Liu, Siwei Ma, Chunjing Xu, Chao Xu, and Wen Gao. Pre-trained image processing transformer. In *Proceedings of the IEEE/CVF Conference on Computer Vision and Pattern Recognition (CVPR)*, pages 12299–12310, 2021. 8
- [6] Liangyu Chen, Xiaojie Chu, X. Zhang, and Jian Sun. Simple baselines for image restoration. In *European Conference on Computer Vision*, 2022. 8
- [7] Shiyang Chen, Jiyuan Zhang, Zhaofei Yu, and Tiejun Huang. Exploring efficient asymmetric blind-spots for self-supervised denoising in real-world scenarios. In *2024 IEEE/CVF Conference on Computer Vision and Pattern Recognition (CVPR)*, pages 2814–2823, 2024. 8
- [8] Sung-Jin Cho, Seoyoun Ji, Jun-Pyo Hong, Seung-Won Jung, and Sung-Jea Ko. Rethinking coarse-to-fine approach in single image deblurring. *2021 IEEE/CVF International Conference on Computer Vision (ICCV)*, pages 4621–4630, 2021. 8
- [9] Kostadin Dabov, Alessandro Foi, Vladimir Katkovnik, and Karen Egiazarian. Image denoising by sparse 3-d transform-domain collaborative filtering. *IEEE Transactions on Image Processing*, 16(8):2080–2095, 2007. 3
- [10] Tao Dai, Jianrui Cai, Yongbing Zhang, Shu-Tao Xia, and Lei Zhang. Second-order attention network for single image super-resolution. In *2019 IEEE/CVF Conference on Computer Vision and Pattern Recognition (CVPR)*, pages 11057–11066, 2019. 1, 8
- [11] Keyan Ding, Kede Ma, Shiqi Wang, and Eero P. Simoncelli. Image quality assessment: Unifying structure and texture similarity. *IEEE Transactions on Pattern Analysis and Machine Intelligence*, 44(5):2567–2581, 2022. 1, 2, 3, 7
- [12] Max Ehrlich, Ser-Nam Lim, Larry S. Davis, and Abhinav Shrivastava. Quantization guided jpeg artifact correction. In *European Conference on Computer Vision*, 2020. 8
- [13] Michael Elad and Michal Aharon. Image denoising via sparse and redundant representations over learned dictionaries. *IEEE Transactions on Image Processing*, 15(12):3736–3745, 2006. 3
- [14] Jinjin Gu, Haoming Cai, Haoyu Chen, Xiaoxing Ye, Jimmy S. J. Ren, and Chao Dong. Pipal: a large-scale image quality assessment dataset for perceptual image restoration. In *European Conference on Computer Vision*, 2020. 6
- [15] Jiayi Jiang, Kai Zhang, and Radu Timofte. Towards flexible blind jpeg artifacts removal. In *2021 IEEE/CVF International Conference on Computer Vision (ICCV)*, pages 4977–4986, 2021. 8
- [16] Daisuke Kiku, Yusuke Monno, Masayuki Tanaka, and Masatoshi Okutomi. Beyond color difference: Residual interpolation for color image demosaicking. *IEEE Transactions on Image Processing*, 25(3):1288–1300, 2016. 1, 8
- [17] Eric C. Larson and Damon M. Chandler. Most apparent distortion: full-reference image quality assessment and the role of strategy. *J. Electronic Imaging*, 19:011006, 2010. 6
- [18] Dasong Li, Xiaoyu Shi, Yi Zhang, Ka Chun Cheung, Simon See, Xiaogang Wang, Hongwei Qin, and Hongsheng Li. A simple baseline for video restoration with grouped spatial-temporal shift. In *2023 IEEE/CVF Conference on Computer Vision and Pattern Recognition (CVPR)*, pages 9822–9832, 2023. 1
- [19] Junyi Li, Zhilu Zhang, Xiaoyu Liu, Chaoyu Feng, Xiaotao Wang, Lei Lei, and Wangmeng Zuo. Spatially adaptive self-supervised learning for real-world image denoising. *2023 IEEE/CVF Conference on Computer Vision and Pattern Recognition (CVPR)*, pages 9914–9924, 2023. 8
- [20] Yawei Li, Yuchen Fan, Xiaoyu Xiang, Denis Demandolx, Rakesh Ranjan, Radu Timofte, and Luc Gool. Efficient and explicit modelling of image hierarchies for image restoration. pages 18278–18289, 2023. 8
- [21] Jingyun Liang, Jie Zhang Cao, Guolei Sun, Kai Zhang, Luc Van Gool, and Radu Timofte. Swinir: Image restoration using swin transformer. *arXiv preprint arXiv:2108.10257*, 2021. 8
- [22] Jie Liang, Hui Zeng, and Lei Zhang. Efficient and degradation-adaptive network for real-world image super-resolution. In *European Conference on Computer Vision*, 2022. 6
- [23] Jie Liang, Huiyu Zeng, and Lei Zhang. Details or artifacts: A locally discriminative learning approach to realistic image super-resolution. *2022 IEEE/CVF Conference on Computer Vision and Pattern Recognition (CVPR)*, pages 5647–5656, 2022. 6
- [24] Xin Yu Lin, Jingwen He, Zi-Yuan Chen, Zhaoyang Lyu, Ben Fei, Bo Dai, Wanli Ouyang, Y. Qiao, and Chao Dong. Diffbir: Towards blind image restoration with generative diffusion prior. *ArXiv*, abs/2308.15070, 2023. 1, 6, 8
- [25] Yang Liu, Zhenyue Qin, Saeed Anwar, Pan Ji, Dongwoo Kim, Sabrina Caldwell, and Tom Gedeon. Invertible denoising network: A light solution for real noise removal. In *2021 IEEE/CVF Conference on Computer Vision and Pattern Recognition (CVPR)*, pages 13360–13369, 2021. 8
- [26] Anish Mittal, Anush Krishna Moorthy, and Alan Conrad Bovik. No-reference image quality assessment in the spatial domain. *IEEE Transactions on Image Processing*, 21(12):4695–4708, 2012. 2, 3
- [27] Ben Niu, Weilei Wen, Wenqi Ren, Xiangde Zhang, Lianping Yang, Shuzhen Wang, Kaihao Zhang, Xiaochun Cao, and

- Haifeng Shen. *Single Image Super-Resolution via a Holistic Attention Network*, pages 191–207. 2020. 1, 8
- [28] Yizhong Pan, Xiao Liu, Xiangyu Liao, Yuanzhouhan Cao, and Chao Ren. Random sub-samples generation for self-supervised real image denoising. *2023 IEEE/CVF International Conference on Computer Vision (ICCV)*, pages 12116–12125, 2023. 8
- [29] Dongwon Park, Dong un Kang, Jisoo Kim, and Se Young Chun. Multi-temporal recurrent neural networks for progressive non-uniform single image deblurring with incremental temporal training. In *European Conference on Computer Vision*, 2019. 8
- [30] Nikolay Ponomarenko, Lina Jin, Oleg Ieremeiev, Vladimir Lukin, Karen Egiazarian, Jaakko Astola, Benoit Vozel, Kacem Chehdi, Marco Carli, Federica Battisti, and C.-C. Jay Kuo. Image database tid2013: Peculiarities, results and perspectives. *Signal Processing: Image Communication*, 30: 57–77, 2015. 6
- [31] Nikolay N. Ponomarenko, Vladimir V. Lukin, and Alexander A. Zelensky. Tid2008 – a database for evaluation of full-reference visual quality assessment metrics. 2004. 6
- [32] Ekta Prashnani, Hong Cai, Yasamin Mostofi, and Pradeep Sen. Pieapp: Perceptual image-error assessment through pairwise preference. In *2018 IEEE/CVF Conference on Computer Vision and Pattern Recognition*, pages 1808–1817, 2018. 6
- [33] Robin Rombach, A. Blattmann, Dominik Lorenz, Patrick Esser, and Björn Ommer. High-resolution image synthesis with latent diffusion models. *2022 IEEE/CVF Conference on Computer Vision and Pattern Recognition (CVPR)*, pages 10674–10685, 2021. 6
- [34] H.R. Sheikh and A.C. Bovik. Image information and visual quality. *IEEE Transactions on Image Processing*, 15(2):430–444, 2006. 4
- [35] H.R. Sheikh, M.F. Sabir, and A.C. Bovik. A statistical evaluation of recent full reference image quality assessment algorithms. *IEEE Transactions on Image Processing*, 15(11): 3440–3451, 2006. 6
- [36] Rajiv Soundararajan and Alan C. Bovik. Rred indices: Reduced reference entropic differencing for image quality assessment. *IEEE Transactions on Image Processing*, 21(2): 517–526, 2012. 3
- [37] Martin J. Wainwright, Eero P. Simoncelli, and Alan S. Willsky. Random cascades on wavelet trees and their use in analyzing and modeling natural images. *Applied and Computational Harmonic Analysis*, 11(1):89–123, 2001. 4
- [38] Jianyi Wang, Zongsheng Yue, Shangchen Zhou, Kelvin C.K. Chan, and Chen Change Loy. Exploiting diffusion prior for real-world image super-resolution. 2024. 1, 6, 8
- [39] Xintao Wang, Liangbin Xie, Chao Dong, and Ying Shan. Real-esrgan: Training real-world blind super-resolution with pure synthetic data. In *2021 IEEE/CVF International Conference on Computer Vision Workshops (ICCVW)*, pages 1905–1914, 2021. 1, 4, 6, 8
- [40] Yinhuai Wang, Jiwen Yu, and Jian Zhang. Zero-shot image restoration using denoising diffusion null-space model. *ArXiv*, abs/2212.00490, 2022. 3, 4
- [41] Zhou Wang, A.C. Bovik, H.R. Sheikh, and E.P. Simoncelli. Image quality assessment: from error visibility to structural similarity. *IEEE Transactions on Image Processing*, 13(4): 600–612, 2004. 1, 2, 3, 7
- [42] Jinjian Wu, Weisi Lin, Guangming Shi, Leida Li, and Yuming Fang. Orientation selectivity based visual pattern for reduced-reference image quality assessment. *Information Sciences*, 351:18–29, 2016. 3
- [43] Rongyuan Wu, Tao Yang, Lingchen Sun, Zhengqiang Zhang, Shuai Li, and Lei Zhang. Seesr: Towards semantics-aware real-world image super-resolution. In *2024 IEEE/CVF Conference on Computer Vision and Pattern Recognition (CVPR)*, pages 25456–25467, 2024. 1, 6, 8
- [44] Tianyi Wu, Sheng Tang, Rui Zhang, Juan Cao, and Yongdong Zhang. Cgnet: A light-weight context guided network for semantic segmentation. *IEEE Transactions on Image Processing*, 30:1169–1179, 2021. 8
- [45] Sidi Yang, Tianhe Wu, Shu Shi, Shan Gong, Ming Cao, Jiahao Wang, and Yujiu Yang. Maniqa: Multi-dimension attention network for no-reference image quality assessment. *2022 IEEE/CVF Conference on Computer Vision and Pattern Recognition Workshops (CVPRW)*, pages 1190–1199, 2022. 2, 3
- [46] Tao Yang, Peiran Ren, Xuansong Xie, and Lei Zhang. Pixel-aware stable diffusion for realistic image super-resolution and personalized stylization. *ArXiv*, abs/2308.14469, 2023. 6
- [47] Zongsheng Yue, Hongwei Yong, Qian Zhao, Lei Zhang, and Deyu Meng. Variational denoising network: Toward blind noise modeling and removal. *ArXiv*, abs/1908.11314, 2019. 8
- [48] Zongsheng Yue, Qian Zhao, Lei Zhang, and Deyu Meng. Dual adversarial network: Toward real-world noise removal and noise generation, 2020. 8
- [49] Zongsheng Yue, Jianyi Wang, and Chen Change Loy. Resshift: Efficient diffusion model for image super-resolution by residual shifting. *ArXiv*, abs/2307.12348, 2023. 6
- [50] Syed Waqas Zamir, Aditya Arora, Salman Khan, Munawar Hayat, Fahad Shahbaz Khan, and Ming Hsuan Yang. Restormer: Efficient transformer for high-resolution image restoration. In *Proceedings - 2022 IEEE/CVF Conference on Computer Vision and Pattern Recognition, CVPR 2022*, pages 5718–5729, United States, 2022. IEEE Computer Society. 6, 8
- [51] Syed Waqas Zamir, Aditya Arora, Salman Khan, Munawar Hayat, Fahad Shahbaz Khan, Ming-Hsuan Yang, and Ling Shao. Multi-stage progressive image restoration. In *2021 IEEE/CVF Conference on Computer Vision and Pattern Recognition (CVPR)*, pages 14816–14826, 2021. 8
- [52] Hongguang Zhang, Yuchao Dai, Hongdong Li, and Piotr Koniusz. Deep stacked hierarchical multi-patch network for image deblurring. In *2019 IEEE/CVF Conference on Computer Vision and Pattern Recognition (CVPR)*, pages 5971–5979, 2019. 8
- [53] Huicong Zhang, Haozhe Xie, and Hongxun Yao. Blur-aware spatio-temporal sparse transformer for video deblurring.

- ring. *2024 IEEE/CVF Conference on Computer Vision and Pattern Recognition (CVPR)*, pages 3616–3626, 2024. 1
- [54] Kai Zhang, Jingyun Liang, Luc Van Gool, and Radu Timofte. Designing a practical degradation model for deep blind image super-resolution. In *IEEE International Conference on Computer Vision*, pages 4791–4800, 2021. 1, 6, 8
- [55] Kai Zhang, Yawei Li, Jingyun Liang, Jiezhong Cao, Yulun Zhang, Hao Tang, Radu Timofte, and Luc Gool. Practical blind denoising via swin-conv-unet and data synthesis, 2022. 6, 8
- [56] Kai Zhang, Yawei Li, Wangmeng Zuo, Lei Zhang, Luc Van Gool, and Radu Timofte. Plug-and-play image restoration with deep denoiser prior. *IEEE Transactions on Pattern Analysis and Machine Intelligence*, 44(10):6360–6376, 2022. 3, 4
- [57] Kai Zhang, Yawei Li, Wangmeng Zuo, Lei Zhang, Luc Van Gool, and Radu Timofte. Plug-and-play image restoration with deep denoiser prior. *IEEE Transactions on Pattern Analysis and Machine Intelligence*, 44(10):6360–6376, 2022. 1, 8
- [58] Lin Zhang, Lei Zhang, and Alan C. Bovik. A feature-enriched completely blind image quality evaluator. *IEEE Transactions on Image Processing*, 24(8):2579–2591, 2015. 2, 3
- [59] Richard Zhang, Phillip Isola, Alexei A Efros, Eli Shechtman, and Oliver Wang. The unreasonable effectiveness of deep features as a perceptual metric. In *CVPR*, 2018. 6
- [60] Richard Zhang, Phillip Isola, Alexei A. Efros, Eli Shechtman, and Oliver Wang. The unreasonable effectiveness of deep features as a perceptual metric. In *2018 IEEE/CVF Conference on Computer Vision and Pattern Recognition*, pages 586–595, 2018. 1, 2, 3, 6, 7
- [61] Yulun Zhang, Kunpeng Li, Kai Li, Lichen Wang, Bineng Zhong, and Yun Fu. Image super-resolution using very deep residual channel attention networks. In *Computer Vision – ECCV 2018: 15th European Conference, Munich, Germany, September 8–14, 2018, Proceedings, Part VII*, page 294–310, Berlin, Heidelberg, 2018. Springer-Verlag. 1, 8
- [62] Fei Zhou, Rongguo Yao, Bozhi Liu, and Guoping Qiu. Visual quality assessment for super-resolved images: Database and method. *IEEE Transactions on Image Processing*, 28(7): 3528–3541, 2019. 6
- [63] Yuanzhi Zhu, K. Zhang, Jingyun Liang, Jiezhong Cao, Bihan Wen, Radu Timofte, and Luc Van Gool. Denoising diffusion models for plug-and-play image restoration. *2023 IEEE/CVF Conference on Computer Vision and Pattern Recognition Workshops (CVPRW)*, pages 1219–1229, 2023. 3, 4

CDI: Blind Image Restoration Fidelity Evaluation based on Consistency with Degraded Image

Supplementary Material

8. Image Restoration Algorithm of Figure.2

Given:

$$\begin{aligned} k &= \text{Kernel} (\text{size} = 9 \times 9, \sigma = 5) \\ I_y &= \text{conv} (I_x, k) \end{aligned} \quad (15)$$

Using existing BIR algorithms to restore I_y :

$$I_{t0} = \text{BIR} (I_y) \quad (16)$$

Design Loss function:

$$L = \|\text{conv} (I_t, k) - I_y\| + \lambda \|I_t - I_{t0}\| \quad (17)$$

Set I_{t0} as the initial value of I_t . Use gradient descent to minimize L and update I_t . In formula.17, $\lambda \|I_t - I_{t0}\|$ is the regularization term, $\lambda \in [0.001, 0.01]$.

9. Image Restoration Algorithm of Figure.3

Given:

$$\begin{aligned} k_1 &= \text{Kernel} (\text{size} = 13 \times 13, \sigma = 1.0) \\ k_2 &= \text{Kernel} (\text{size} = 13 \times 13, \sigma = 1.06 \text{ or } 1.12 \text{ or } 1.18) \\ I_y &= \text{conv} (I_x, k_1) \end{aligned} \quad (18)$$

Design Loss function:

$$L = \|\text{conv} (I_t, k_2) - I_y\| + \lambda \|I_t - I_x\| \quad (19)$$

Set I_x as the initial value of I_t . Use gradient descent to minimize L and update I_t . In formula.19, $\lambda \|I_t - I_x\|$ is the regularization term, $\lambda \in [0.001, 0.01]$.

10. Proof of RGCDI Property

Idempotency. Multiple WAE operations are equivalent to a single one.

Given:

$$\begin{aligned} x &= \text{DWT} [I_x] \\ y &= \text{DWT} [I_y] \\ \mu_A &= \text{COV} (y, x) / \text{COV} (x, x) \\ \sigma_n^2 &= \text{COV} (y, y) - \mu_A \text{COV} (y, x) \\ \mu_N &= \left(I + \frac{\sigma_n^2}{\mu_A^2} \text{COV} (x, x)^{-1} \right)^{-1} \\ \text{DWT} [\text{WAE} (I_x, I_y)] &= \mu_N \mu_A x \\ \text{WAE} (I_x, I_y) &= \text{IDWT} (\mu_N \mu_A x) \end{aligned} \quad (20)$$

Calculating $\text{WAE} (I_x, \text{WAE} (I_x, I_y))$:

$$\begin{aligned} \text{WNS} (x, \mu_N \mu_A x) &= x * \text{COV} (x, \mu_N \mu_A x) / \text{COV} (x, x) \\ \text{WNS} (x, \mu_N \mu_A x) &= \mu_N \mu_A x \\ \text{WNEA} (\mu_N \mu_A x, 0) &= \mu_N \mu_A x \\ \text{DWT} [\text{WAE} (I_x, \text{WAE} (I_x, I_y))] &= \mu_N \mu_A x \\ \text{DWT} [\text{WAE} (I_x, \text{WAE} (I_x, I_y))] &= \text{DWT} [\text{WAE} (I_x, I_y)] \\ \text{WAE} (I_x, \text{WAE} (I_x, I_y)) &= \text{WAE} (I_x, I_y) \end{aligned} \quad (21)$$

Calculating $\text{WAE} (\text{WAE} (I_x, I_y), I_y)$:

$$\begin{aligned} \text{WNS} (\mu_N \mu_A x, y) &= \frac{\mu_N \mu_A x * \text{COV} (\mu_N \mu_A x, y)}{\text{COV} (\mu_N \mu_A x, \mu_N \mu_A x)} \\ \text{WNS} (\mu_N \mu_A x, y) &= x * \text{COV} (x, y) / \text{COV} (x, x) \\ \text{WNS} (\mu_N \mu_A x, y) &= \mu_A x \\ \text{WNEA} (\mu_A x, y - \mu_A x) &= \mu_N \mu_A x \\ \text{DWT} [\text{WAE} (\text{WAE} (I_x, I_y), I_y)] &= \text{DWT} [\text{WAE} (I_x, I_y)] \\ \text{WAE} (\text{WAE} (I_x, I_y), I_y) &= \text{WAE} (I_x, I_y) \end{aligned} \quad (22)$$

WAE and Degradation Cascade Exchangeability. The WAE of cascading multiple degradations is equivalent to cascading multiple WAEs of a single degradation.

Given:

$$\begin{aligned} x &= \text{DWT} [I_x] \\ y_1 &= \text{DWT} [D_1 (I_x)] \\ \mu_{A1} &= \text{COV} (y_1, x) / \text{COV} (x, x) \\ \sigma_{n1}^2 &= \text{COV} (y_1, y_1) - \mu_{A1} \text{COV} (y_1, x) \\ \mu_{N1} &= \left(I + \frac{\sigma_{n1}^2}{\mu_{A1}^2} \text{COV} (x, x)^{-1} \right)^{-1} \\ \text{DWT} [\text{WAE} (I_x, D_1 (I_x))] &= \mu_{N1} \mu_{A1} x \\ \text{WAE} (I_x, D_1 (I_x)) &= \text{IDWT} (\mu_{N1} \mu_{A1} x) \\ y_2 &= \text{DWT} [D_2 (D_1 (I_x))] \\ \mu_{A2} &= \text{COV} (y_2, x) / \text{COV} (x, x) \\ \sigma_{n2}^2 &= \text{COV} (y_2, y_2) - \mu_{A2} \text{COV} (y_2, x) \\ \mu_{N2} &= \left(I + \frac{\sigma_{n2}^2}{\mu_{A2}^2} \text{COV} (x, x)^{-1} \right)^{-1} \\ \text{DWT} [\text{WAE} (I_x, D_2 (D_1 (I_x)))] &= \mu_{N2} \mu_{A2} x \\ \text{WAE} (I_x, D_2 (D_1 (I_x))) &= \text{IDWT} (\mu_{N2} \mu_{A2} x) \end{aligned} \quad (23)$$

		RCAN	SAN	HAN	IPT	SwinIR	GRL-S
BSD100	x2	40.00 / 0.14	40.00 / 0.14	40.00 / 0.14	40.00 / 0.13	40.00 / 0.12	40.00 / 0.13
	x4	39.95 / 0.25	39.96 / 0.23	39.97 / 0.22	39.95 / 0.24	39.95 / 0.19	39.75 / 0.29
Manga109	x2	39.97 / 0.02	39.98 / 0.02	39.97 / 0.02	39.97 / 0.02	39.97 / 0.03	39.97 / 0.03
	x4	39.80 / 0.14	39.82 / 0.12	39.82 / 0.13	39.79 / 0.14	39.74 / 0.19	39.76 / 0.17

Table 8. **RACDI Test Results, Classic SR on BSD100 and Manga109**: For each cell of data in this table, the number on the left represents RACDI_PSNR and the number on the right represents the mean error of RACDI_PSNR relative to RGCDI_PSNR. Maximum Mean Error 0.29dB

		DnCNN	IPT	DRUNet	SwinIR	Restormer	SCUNet
CBSD68	$\sigma = 15$	39.79 / 2.28	-	39.88 / 2.03	40.00 / 2.06	39.88 / 1.95	39.90 / 1.95
	$\sigma = 25$	39.11 / 2.49	-	39.54 / 2.47	40.00 / 2.86	39.54 / 2.39	39.60 / 2.43
	$\sigma = 50$	36.85 / 1.66	33.70 / 2.31	37.98 / 1.91	39.93 / 3.71	37.92 / 1.85	38.08 / 1.89
McMaster	$\sigma = 15$	38.68 / 1.29	-	39.59 / 0.76	40.00 / 1.03	39.61 / 0.65	39.64 / 0.68
	$\sigma = 25$	38.04 / 1.47	-	39.08 / 1.13	40.00 / 1.92	39.12 / 1.01	39.16 / 1.05
	$\sigma = 50$	36.10 / 1.17	34.66 / 1.79	37.76 / 1.19	39.94 / 3.21	37.78 / 1.04	37.86 / 1.10

Table 9. **RACDI Test Results, Gaussian Noise on CBS68 and McMaster**: For each cell of data in this table, the number on the left represents RACDI_PSNR and the number on the right represents the mean error of RACDI_PSNR relative to RGCDI_PSNR. Maximum Mean Error 3.71dB

Calculating $WAE(WAE(I_x, D_1(I_x)), D_2(D_1(I_x)))$:

$$\begin{aligned}
WNS(\mu_{N1}\mu_{A1}x, y_2) &= \frac{\mu_{N1}\mu_{A1}x * COV(\mu_{N1}\mu_{A1}x, y_2)}{COV(\mu_{N1}\mu_{A1}x, \mu_{N1}\mu_{A1}x)} \\
WNS(\mu_{N1}\mu_{A1}x, y_2) &= x * COV(x, y_2) / COV(x, x) \\
WNS(\mu_{N1}\mu_{A1}x, y_2) &= \mu_{A2}x \\
WNEA(\mu_{A2}x, y_2 - \mu_{A2}x) &= \mu_{N2}\mu_{A2}x \\
DWT[WAE(WAE(I_x, D_1(I_x)), D_2(D_1(I_x)))] \\
&= DWT[WAE(I_x, D_2(D_1(I_x)))] \\
WAE(WAE(I_x, D_1(I_x)), D_2(D_1(I_x))) \\
&= WAE(I_x, D_2(D_1(I_x)))
\end{aligned} \tag{24}$$

		QGAC	FBCNN	GRL-S
LIVE1	QF10	38.55 / 5.85	39.43 / 6.47	39.35 / 5.87
	QF20	39.29 / 4.78	39.77 / 4.93	39.69 / 4.37
	QF30	39.47 / 4.13	39.84 / 4.17	39.74 / 3.57
	QF40	39.58 / 3.80	39.88 / 3.77	39.79 / 3.18

Table 10. **RACDI Test Results, CDIPSNR, JPEG Compression on LIVE1**: For each cell of data in this table, the number on the left represents RACDI_PSNR and the number on the right represents the mean error of RACDI_PSNR relative to RGCDI_PSNR. Maximum Mean Error 6.47dB

RGCDI_PSNR \geq PSNR (Conditional). In general, the attenuation coefficients satisfy $0 \leq \mu_N\mu_A \leq 1$, and the differences between degraded images is smaller than that of the original images.

Given:

$$\begin{aligned}
x &= DWT[I_x] \\
y &= DWT[I_y] \\
t &= DWT[I_t] \\
\mu_A &= COV(y, x) / COV(x, x) \\
\sigma_n^2 &= COV(y, y) - \mu_A COV(y, x) \\
\mu_N &= \left(I + \frac{\sigma_n^2}{\mu_A^2} COV(x, x) \right)^{-1} \\
DWT(I_{\tilde{y}}) &= \mu_N \mu_A x \\
\mu_M &= \arg \min_{\mu_M} \|\mu_M t - \mu_N \mu_A x\| \\
DWT(I_{\tilde{t}}) &= \mu_M t
\end{aligned} \tag{25}$$

Calculating $\|I_{\tilde{t}} - I_{\tilde{y}}\|$: (Note: Wavelet transform adopts an orthogonal wavelet basis.)

$$\begin{aligned}
\|I_{\tilde{t}} - I_{\tilde{y}}\| &= \|DWT(I_{\tilde{t}}) - DWT(I_{\tilde{y}})\| \\
&= \|\mu_M t - \mu_N \mu_A x\| \\
&\leq \|\mu_N \mu_A t - \mu_N \mu_A x\| \\
&= \mu_N^2 \mu_A^2 \|t - x\|
\end{aligned} \tag{26}$$

Assume: $\mu_N \mu_A \leq 1$

$$\begin{aligned}
\|I_{\tilde{t}} - I_{\tilde{y}}\| &\leq \|t - x\| \\
&= \|IDWT(t) - IDWT(x)\| \\
&= \|I_t - I_x\|
\end{aligned} \tag{27}$$

$$\begin{aligned}
10 \log(255^2 / \|I_{\tilde{t}} - I_{\tilde{y}}\|) &\geq 10 \log(255^2 / \|I_t - I_x\|) \\
RGCDI_PSNR(I_t, I_x) &\geq PSNR(I_t, I_x)
\end{aligned} \tag{28}$$

11. RACDI Testing (Supplementary Experimental Results)

We apply SCUNet as the WAENet backbone network, and test the RACDI on more Datasets. Table.8 shows RACDI test for Classic SR on the BSD100 and Manga109 datasets. Similar to the results on the Urban100 dataset, the maximum mean error is very small, only reaching 0.29dB. Table.9 shows RACDI test for Gaussian De-noise on the CBS68 and McMaster datasets. Similar to the results on the Urban100 dataset, the maximum mean error is moderate, reaching 3.71dB. Table.10 shows RACDI test for JPEG Restoration on the LIVE1 dataset. Similar to the results on the BSDS500 dataset, the maximum mean error is larger, reaching 6.47dB.